Multilinear Slicing for curve resolution of fluorescence imaging with sequential illumination

Dario Cevoli, Siewert Hugelier, Robin van den Eynde, Olivier Devos, Peter Dedecker, Cyril Ruckebusch

Talanta 241 (2022) 123231

Contents lists available at ScienceDirect

Talanta

journal homepage: www.elsevier.com/locate/talanta

Multilinear Slicing for curve resolution of fluorescence imaging with sequential illumination

Dario Cevoli [a,b], Siewert Hugelier [b], Robin Van den Eynde [b], Olivier Devos [a], Peter Dedecker [b], Cyril Ruckebusch [a,*]

[a] Univ. Lille, CNRS, LASIRE, Laboratory of Advanced Spectroscopy, Interactions, Reactivity and Environment, F-59000, Lille, France
[b] KU Leuven, Laboratory for NanoBiology, Department of Chemistry, Celestijnenlaan 200G, 3001, Heverlee, Leuven, Belgium

ARTICLE INFO

Keywords:
Fluorescence microscopy
Exponential decays
Unmixing
Multiway analysis
Slicing
PARAFAC
MCR-ALS

ABSTRACT

Fluorescence microscopy is an extremely powerful technique that allows to distinguish multiple labels based on their emission color or other properties, such as their photobleaching and fluorescence recovery kinetics. These kinetics are ideally assumed to be mono-exponential in nature, where the time constants intrinsic to each fluorophore can be used to quantify their presence in the sample. However, these time constants also depend on the specifics of the illumination and sample conditions, meaning that identifying the different contributions in a mixture using a single-channel detection may not be straightforward. In this work, we propose a factor analysis approach called Slicing to identify the different contributions in a multiplexed fluorescence microscopy image exploiting a single measurement channel. With Slicing, a two-way dataset is rearranged into a three-way dataset, which allows the application of a trilinear decomposition model to derive individual profiles for all the model components. We demonstrate this method on bleaching - recovery fluorescence microscopy imaging data of U2OS cells, allowing us to determine the spatial distribution of the dyes and their associated characteristic relaxation traces, without relying on a parametric fitting. By requiring little *a priori* knowledge and efficiently handling perturbation factors, our method represents a general approach for the recovery of multiple mono-exponential profiles from single-channel microscopy data.

1. Introduction

Fluorescence imaging is a well known and widely used technique in life sciences, because of its non-destructivity and selectivity. A limiting factor for the technique is the difficulty with which several fluorescent labels can be visualised at once. For this reason many techniques have been developed that focus on the separation of signals from different labels recorded simultaneously, e.g. using differences in their spectral signature or in their temporal dynamics [1–3]. In the recent work by Hugelier et al. [4] the signal of two probes have been successfully unmixed based on their temporal dynamics: U2OS cells stained with $DiBAC_4(3)$ and Concanavalin A - Alexa Fluor 488 were analyzed with a sequential illumination strategy where a first photodestruction phase was followed by a fluorescence recovery period. The two dyes exhibit similar spectral signatures (thus cannot be separated using different color channels) but have different recovery behaviours, allowing three different cellular structures to be separated from a single-channel measurement using factor analysis.

Multi-exponential analysis has seen a long history in exploratory data analysis and curve resolution approaches. In 1997, Windig and Antalek [5] introduced a method called direct exponential curve resolution analysis (DECRA) to resolve series of NMR mixture spectra in which the contribution of the components varies with a decaying exponential. The proposed approach exploits the natural property of exponential curves to be proportional to the lagged version of themselves, a procedure that was later denominated Slicing [6]. This procedure makes it possible to add a new pseudo-dimension to the measured two-way data set and decompose the resulting three-way data set using trilinear methods such as direct trilinear decomposition (DTLD) [7] and parallel factor analysis (PARAFAC) [8]. This strategy has also been successfully used for multivariate curve resolution - alternating least squares (MCR-ALS) in the recent work by Devos et al. [9] to unmix time-resolved emission spectroscopy data of a photoswitchable fluorescence protein. A key feature of MCR Slicing is the ability to create

* Corresponding author.
E-mail address: cyril.ruckebusch@univ-lille.fr (C. Ruckebusch).

https://doi.org/10.1016/j.talanta.2022.123231
Received 13 October 2021; Received in revised form 12 January 2022; Accepted 13 January 2022
Available online 20 January 2022

hybrid models, where trilinearity is enforced only on some of the components or on a subset of the original dataset. The data can therefore be described by a combination of exponential and non-exponential decays, whereas in PARAFAC Slicing, the same assumptions has to be made for all the components in the data.

In this work, we show that the Slicing approach can be applied to photobleaching imaging data for which exponential behavior is assumed for the decaying fluorescence signal. The clear advantage is that it enables the application of multilinear models without requiring in-depth knowledge of the specific system analyzed, yielding a single comprehensive model obtained in a non parametric way. Also, when a multilinear decomposition is applicable, the methodology can often be applied directly with no parameter optimization required by the user other than the selection of number of components, which can be determined using dedicated tools [10]. We demonstrate the applicability of MCR Slicing approaches to the unmixing of sequential illumination fluorescence microscopy imaging data of different levels of complexity. Moreover, if the laser power is controlled during sequential illumination, we show that quadrilinear PARAFAC models can be fitted resulting in a very robust description of the signals' behaviour in the pixel, time and repetition modes. In another illumination scenario, a hybrid bilinear-trilinear MCR Slicing model allows the combined description of both exponentially and non-exponentially decaying contributions, showing that deviation to the ideal exponential behavior occurring when, e.g., analyzing images covering a very large field of view, can be coped with. Overall, multilinear Slicing has an important potential for data analysis and unmixing in fluorescence microscopy imaging with integrative (single-channel) detection.

2. Materials and methods

2.1. Sample preparation

Samples were obtained by adding 1 mL Concanavalin A - Alexa Fluor 488 (ConA) solution (500 μg mL^{-1}; Thermo-Fisher; n° C11252) to a dish of U2OS cells prior to fixation, incubated at 37 °C for 30 min and washed twice with 1 mL Hank's balanced salt solution (HBSS; Gibco; n° 14 065-049). The $DiBAC_4(3)$ was added several minutes before imaging the sample so that an equilibrium could be achieved. 1 mL of a 10 μM $DiBAC_4(3)$ solution (Biotium; n° 61 011) was added after washing with HBSS. This fixation protocol is the same used for the preparation of samples in Ref. [4].

2.2. Imaging

To form an image of these samples, a Nikon Ti-E2 microscope equipped with a × 100 CFI apo TIRF objective, a ZT405/488/561/640rpcv2 dichroic (Chroma) paired with a ZET405/488/561/640 m emission filter (Chroma) and a PCO edge 4.2 CMOS camera was used (virtual pixel size of 118 nm; 1024 × 1024 pixels). As an excitation light source, a 488 nm Oxxius laser was used.

2.3. Measurement schemes

The below described measurement schemes were used to obtain the data; each datapoint was followed by an image acquisition (exposure 30 ms with a laser power setting of 0.17 mW).

Dataset 1: fixed laser power. i) 60 × 0.3 s of photodestruction with 2.23 mW 488 nm laser power (denoted as section A1 in Fig. 2); ii) 10 × 5 s fluorophore recovery; iii) 60 × 0.3 s of photodestruction with 2.23 mW 488 nm laser power (section B1); iv) 30 × 5 s fluorophore recovery; v) 60 × 0.3 s of photodestruction with 2.23 mW 488 nm laser power (section C1).
Dataset 2: increasing laser power. i) 120 × 0.15 s of photodestruction with 0.57 mW 488 nm laser power; ii) 60 × 30 s fluorophore recovery; iii) 120 × 0.15 s of photodestruction with 2.23 mW 488 nm laser power (denoted as section A2 in Fig. 5); iv) 60 × 30 s fluorophore recovery; v) 120 × 0.15 s of photodestruction with 3.91 mW 488 nm laser power (section B2); vi) 60 × 30 s fluorophore recovery; vii) 120 × 0.15 s of photodestruction with 6.2 mW 488 nm laser power (section C2).

For both datasets only the photodestruction parts were used for the data analysis.

2.4. MCR-ALS

MCR-ALS [11] is a bilinear data decomposition algorithm, following the model expressed (element-wise) in Equation (1).

$$d_{i,j} = \sum_{n=1}^{N} c_{i,n} s_{j,n} + e_{i,j} \qquad i = 1\ldots I, j = 1\ldots J \tag{1}$$

Or, more commonly, in its matricial form as in Equation (2).

$$\mathbf{D} = \mathbf{C}\mathbf{S}^{\mathrm{T}} + \mathbf{E} \tag{2}$$

Here **D** is the dataset (with dimensions I rows and J columns); **C** is the (I x N) matrix formed by the N pure contribution across the row mode, $\mathbf{S}^{\mathrm{T}}$ is the (N x J) matrix formed by the N pure contribution across the column mode and **E** is the (I x J) matrix of errors associated to the model. The algorithm is widely used and more in depth information can be found in Ref. [12].

The profiles are optimized alternatingly in **C** and $\mathbf{S}^{\mathrm{T}}$ in an iterative fashion, until a convergence criterion is achieved, usually defined as the stabilization of the lack-of-fit (LOF), as expressed in Equation (3):

$$LOF = \sqrt{\frac{\sum_{i,j} e_{i,j}^2}{\sum_{i,j} d_{i,j}^2}} \tag{3}$$

where $e_{i,j}^2$ and $d_{i,j}^2$ are the $(i \text{ x } j)^{th}$ element of **D** and **E** respectively. Another metric commonly used in conjunction with the LOF is the explained variance, defined as in Equation (4):

$$r^2 = 1 - \frac{\sum e_{i,j}^2}{\sum d_{i,j}^2} = 1 - LOF^2 \tag{4}$$

Constraints, defined as corrections apported to the profiles to conform to specific properties [11], are applied at each iteration. Constraints are decided by the operator and ensure that the solution selected by the optimization is in accordance with the information known about the system. The ability to impose constraints selectively to only some of the components grants a substantial flexibility to the resolution, allowing the user to leverage all the information available on the system [9]. In this work, a non-negativity constraint is always applied to all the components' profiles. We refer to the sections below for the more specific implementation of a trilinearity constraint.

2.5. PARAFAC

PARAFAC [8] is a multilinear factor analysis method that can be considered as a multi-way generalization of the principal component analysis (PCA) for two-way data. For three-way data, the decomposition can be expressed by Equation (5):

$$d_{i,j,k} = \sum_{n=1}^{N} c_{i,n} s_{j,n} p_{k,n} + e_{i,j,k} \qquad i = 1\ldots I, j = 1\ldots J, k = 1\ldots K \tag{5}$$

where $d_{i,j,k}$ is the $(i \text{ x } j \text{ x } k)^{th}$ element of the $\underline{\mathbf{D}}$ datacube; $c_{i,n}$, $s_{j,n}$, and $p_{k,n}$ are the pure contributions across the three modes, and $e_{i,j,k}$ is the $(i \text{ x } j \text{ x } k)^{th}$ error associated to the model. The model can also be written in a matricial form, as in Equation (6), although this is not as common because of its complexity.

$$\underline{\mathbf{D}}^{(I \times JK)} = \mathbf{C}(\mathbf{P} \odot \mathbf{S})^{\mathrm{T}} + \mathbf{E}^{(I \times JK)} \tag{6}$$

Here $\underline{\mathbf{D}}^{(I\times JK)}$ is the matricised form of the datacube (the superscript ($I \times JK$) identifies the way the cube is matricised) and $\odot$ represents the column-wise Khatri-Rao product [13].

PARAFAC decomposition has a few advantages, notably that it is more robust and easier to interpret compared with lower dimensional models needing unfolding [8]. PARAFAC can also be applied to higher dimensional datasets, as in four- or five-way data, with adjustments to the decomposition model provided in Equation (5) and Equation (6). Applications of higher-order decomposition models (e.g. quadrilinear) exist in chemometrics and analytical chemistry [14], however, to our knowledge there has been no result reported on the decomposition and exploratory analysis of fluorescence microscopy imaging data. In the PARAFAC decomposition, in contrast with the aforementioned MCR bilinear decomposition, the problem of rotational ambiguity (model identification) does not exist, given that the analyzed data are indeed multilinear [[15], Chapter 5]. However, the model might be more easily estimated by applying constraint to the loadings [16] and, in this work, PARAFAC is always performed under a non-negativity constraint.

2.6. Slicing

Slicing has been proposed as a method to leverage the intrinsic mathematical properties of exponential decay functions to build multi-way datasets. More specifically, the shifting property of exponential functions is expressed in Equation 7

$$Ae^{-(t+l)/\tau} = Ae^{-t/\tau}e^{-l/\tau} = A'e^{-t/\tau} \tag{7}$$

where l is an arbitrary lag along the time axis. In this way, by applying lags of different durations to an exponential decay signal, the pre-exponential amplitude factor A varies while the characteristic time τ remains constant. This translates into a linear relationship that can be exploited to create a new pseudo-mode. When Slicing is applied to two-way data, different slabs are produced by taking sequential subsets of the matrix: a window of fixed dimension is moved along rows, each time starting at a different column (*i.e.* different temporal lags). The slabs are then concatenated to produce a three-way datacube. Several specific Slicing algorithms have been developed and tested, mostly differentiated by the choice of the specific lags applied. In this work the lags used are equal to the powers of 2 (l = [1, 2, 4, 8 …]), as in the approach proposed in Ref. [17].

2.7. Multilinear Slicing on images

To decompose images applying factor analysis techniques, a preliminary unfolding of the image datacube has to be applied to provide a two-way data set. Slicing is then applied to the unfolded dataset to produce slabs. Once the slabs are created, they can be concatenated either in the slab direction to produce a three-way datacube suitable for PARAFAC decomposition, or in the row direction to produce a row-augmented multiset suitable for MCR Slicing analysis [9]. After unmixing, the concentration profiles obtained can be refolded to get the individual images corresponding to each pure recovered component. Fig. 1 schematizes and summarize this process. In both cases the core trilinearity property will be used for the decomposition, but in the first case by the trilinear model itself (PARAFAC Slicing), while in the second case a constraint of equal shape is applied to the component profiles within each iteration of an MCR-ALS bilinear model (MCR Slicing). The choice between these two alternative approaches should be driven by the data themselves. While a trilinear model is more robust, trilinearity is not always verified in the data and therefore its applicability is more limited compared to a bilinear model. Thus, a clear asset of MCR Slicing for analyzing fluorescence imaging data of complex systems is that it is better suited to handle perturbation factors, since MCR-ALS decomposition model can embed components whose profiles do not show ideal (*i.e.* exponential, in this work) behaviour [18].

3. Results and discussion

The first dataset (Dataset 1) consists of U2OS cells stained with ConA and $DiBAC_4(3)$. The data is shown in Fig. 2. A sequential strategy comprised of alternating periods of photodestruction by laser illumination and fluorescence recovery was applied, and only the sections corresponding to the illumination phases were analyzed (see Materials and Methods). The laser power used for illumination was kept constant. The averaged image of the full field of view is shown in Fig. 2a, while the recovered time traces of the three photodestruction blocks (which we will call A1, B1 and C1) are shown in Fig. 2c.

Each block was individually sliced into five slabs, and then the fifteen slices were concatenated in a row-wise augmented multiblock structure to which MCR Slicing was applied. In Fig. 3, the results of a three-component MCR Slicing decomposition of the multiblock structure are

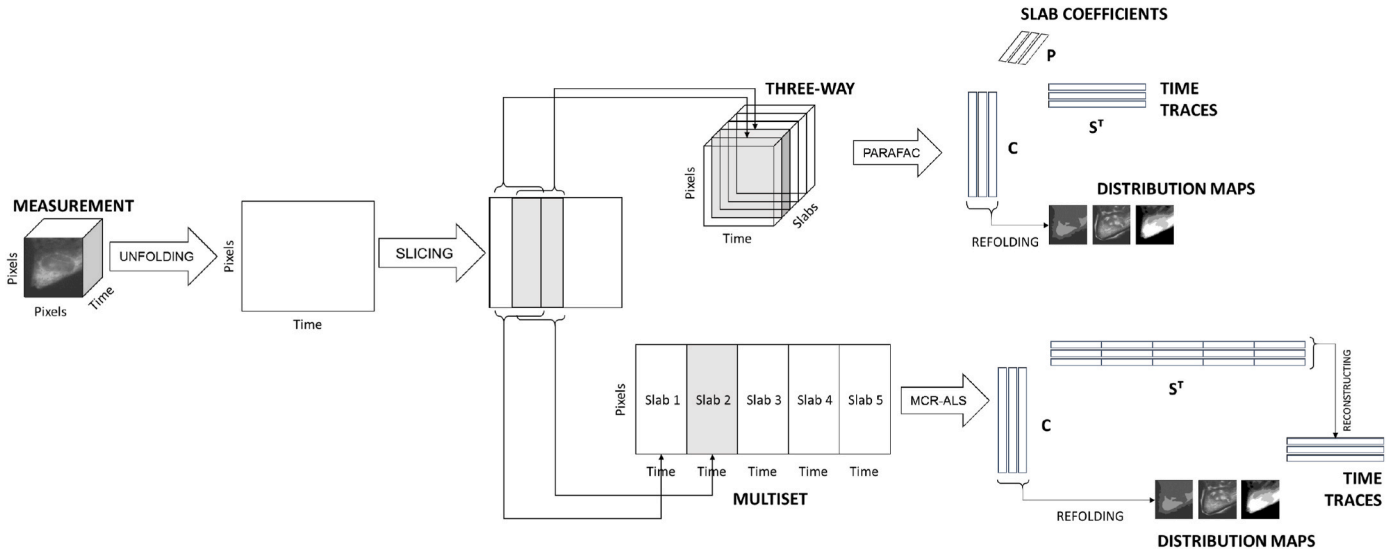

Fig. 1. Schematic representation of Slicing applied to fluorescence imaging data. The image datacube is unfolded by considering each pixel as a different row of a two-way dataset. Slabs are then produced and are rearranged either as a three-way datacube to be decomposed applying PARAFAC or as a two-way multiset data structure analyzed applying MCR Slicing. After refolding, both approaches yield the distribution maps (images) and monoexponential decays of the individual pure components.

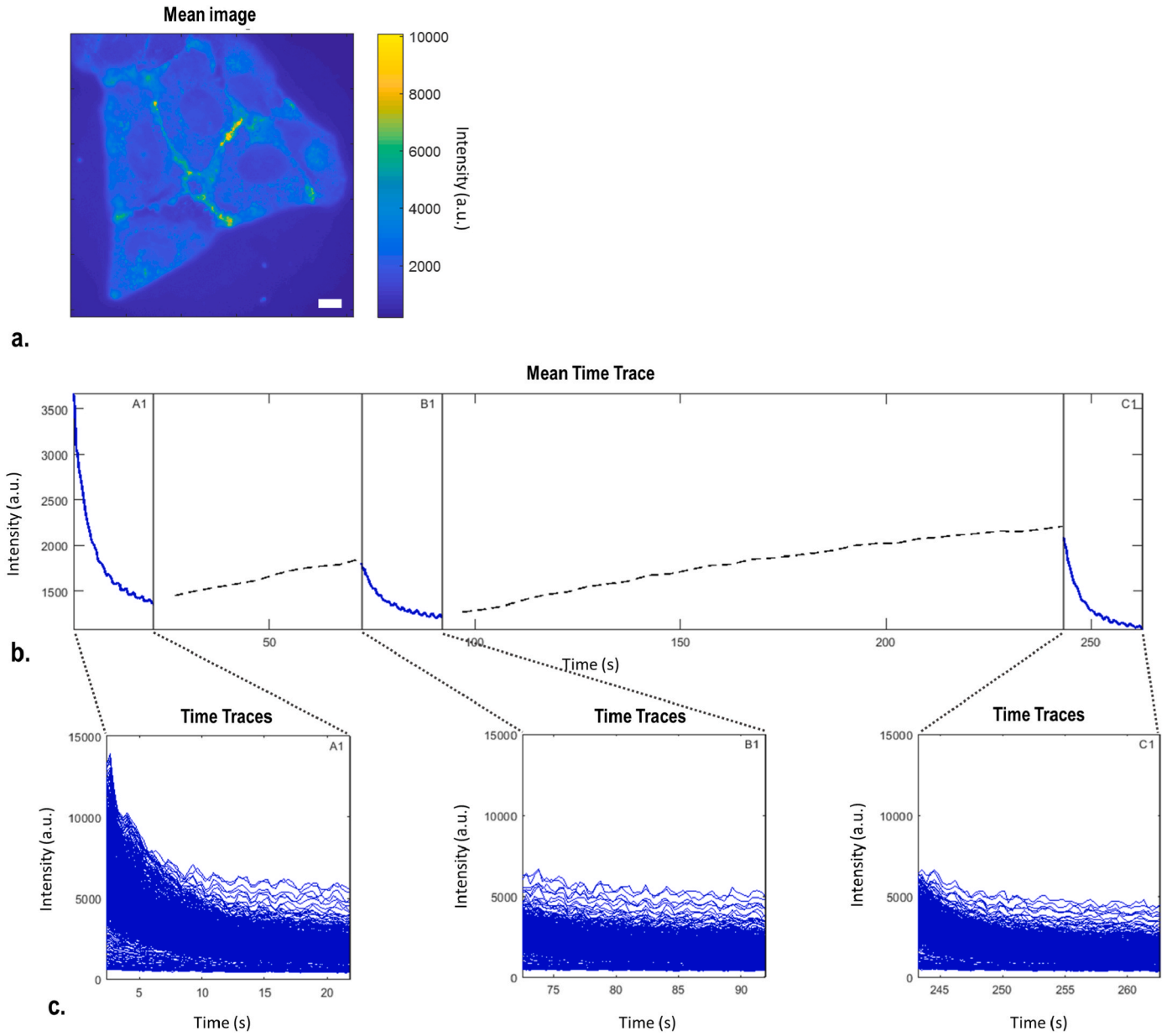

Fig. 2. First dataset of U2OS cells. **a.** Image averaged across all acquisition times. Image size 120 × 120 μm, scalebar 10 μm. **b.** Averaged time traces, shown to illustrate the illumination scheme: three sections of 18 s of photodestruction using 2.23 mW laser power, with 50 s of fluorophore recovery between section A1 and B1, 150 s between B1 and C1. Only the photodestruction sections were used for the analysis. **c.** Time traces relative to the three photodestruction sections.

reported. The images in Fig. 3a–c provide the distribution maps corresponding to the three components extracted. The data in Fig. 3d corresponds to the "reassembled" profiles obtained for the three sections ("raw" results of the MCR Slicing before the rearrangement are added in the Appendix, Fig. 7). These rearranged profiles show clear monoexponential behavior and the overall bleaching behaviour can thus be described by considering three components characterized by monoexponential decaying time profiles (it should be noted that the applied trilinearity constraint forces the profiles to have the same shape, but not necessary an exponential one). Among the three components extracted, the first one (marked in blue) can be clearly distinguished from the other two by its slower destruction rate and by the fact that it shows no recovery, a behaviour that can be attributed to ConA [4]. The image in Fig. 3a confirms this hypothesis, since most of the contribution is found in the space between cells, which can be attributed to an affinity for Lamin [4]. The remaining two components can then be assigned to two different behaviours of the $DiBAC_4(3)$, where the differences in destruction rate are due to influences by the local environment. As previously observed in Ref. [4], the fastest among the two (corresponding to $DiBAC_4(3)$-B in Fig. 3) is mainly localized around the nucleus. Comparing the results obtained in the three blocks (Fig. 3d) it appears clearly that while the characteristic destruction rates corresponding to the three individual components are similar (because of the constant laser power used for the three blocks), the longer recovery time before C1 translates into a higher relative availability of fluorophores, and therefore in a higher response signal compared to B1. Indeed, this reveals that another linear relationship exists within the data which can be leveraged as an added dimension for the model. In practice, this means that a four-dimensional hypercube can be built, where the fourth dimension will be obtained by concatenating the blocks A1 to C1, which can then be decomposed using a quadrilinear PARAFAC model.

We now report the results obtained applying a three-component quadrilinear PARAFAC Slicing model. The uniqueness property of the PARAFAC model results (except for scaling and permutation of the

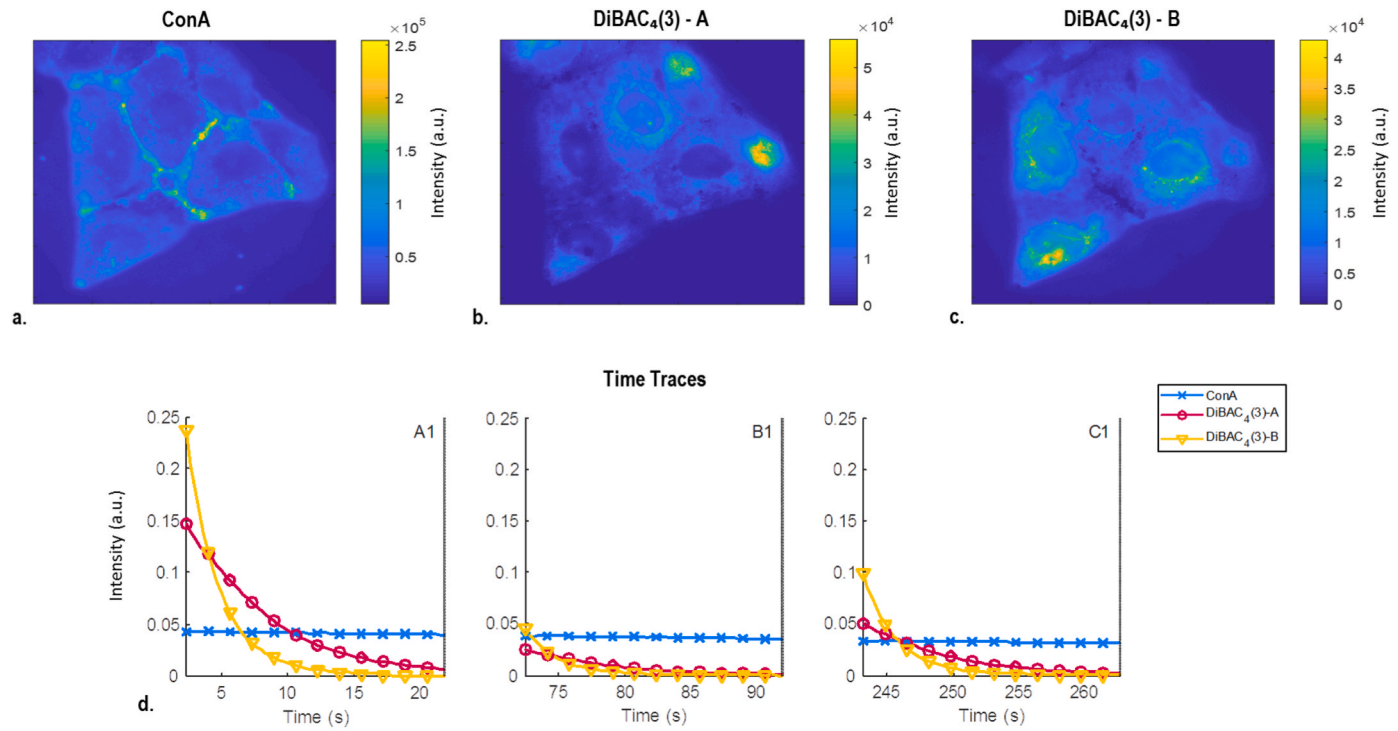

Fig. 3. Three-component MCR Slicing decomposition of Dataset 1. **a-c.** Distribution maps attributed to contribution from ConA (**a**) and DiBAC$_4$(3) (**b-c**) respectively; **d.** Corresponding monoexponential time traces. LOF:4.66%, $r^2 = 99.78\%$.

component matrices) is a key feature and one of the most attractive feature of the method for its applications [15, Chapter 5]. However, as previously mentioned, a quadrilinear model is strict, and slight deviations from the ideal multilinear behaviour of the data will results in the lack of convergence of the model. Due to spatial local differences, one model could not fit the whole field of view of the image. This can be explained by the fact that, ideally, to evaluate the photobleaching rate of fluorescent probes the data should be acquired under strictly identical illumination conditions. However this can always be questioned, in particular when considering large field of view images. To circumvent the issue, patches of the full images were considered. Patching is a commonly used approach to extract spatial features in image processing. We show here that local models constructed on different patches can be more suitable for multilinear modelling in situations where the image suffers from perturbating effects/artifacts such as uneven illumination or out of focus regions. Considering patches of the full images, quadrilinear PARAFAC Slicing models could be fitted locally. It should be noted that, once a patch has been selected, the procedure is automatic and does not necessitate any further input from the operator. Fig. 4 provides the results obtained for a three-component model fitted over four different patches (see Fig. 4a). As previously, five slabs were used. Fore example, for patch 1 Fig. 4b shows the distribution maps for the three components extracted from the first patch, while the relative time traces are shown in Fig. 4c. Again, the slow component (blue trace in 4c) attributed to ConA is distinguishable from the faster components (red and yellow traces in Fig. 4c) attributable to DiBAC$_4$(3), which can be found mostly around the nucleus and the endoplasmic reticulum. The fourth mode of the model is represented in Fig. 4d, where the variation across the three different sections of the recovery rate of each component is described. The first loading of this mode (blue trace in Fig. 4d) clearly confirms the fact that ConA does not recover between successive bleaching periods. On the contrary, the loadings extracted for the two DiBAC$_4$(3) components show again that, when more time is allowed for the dye to recover (50 s recovery time between A1 and B1; 150 s between B1 and C1), more dye is available at the start of the following destruction section. The results displayed in Fig. 4c–j are very similar, with slight variations that can be expected in cell imaging due to local environment, and confirm the proposed interpretation. However, locally, as for the results displayed in Fig. 4k-m, significant deviation to the ideal quadrilinear model can sometimes be observed.

The second dataset (Dataset 2) is another U2OS cell sample stained with ConA and DiBAC$_4$(3) but a different measurement scheme was applied. The data is shown in Fig. 5. The averaged image of the full field of view is shown in Fig. 5a (a smaller region of interest with a particularly visible structure has been chosen) and the recovered time traces of the three photodestruction blocks (this time referred as A2, B2 and C2) are shown in Fig. 5c. In this case, the sequential illumination did not use the same laser power in all the sections, having instead increasingly higher laser powers for each block. For this reason, in contrast with Dataset 1, the characteristic rates constant of each component will not be comparable among the different blocks. Indeed a closer look at Fig. 2c reveals that overall time traces decay faster going from A2 to C2. Hence, no common mode exists between the three blocks and therefore PARAFAC Slicing cannot be used. By contrast, MCR Slicing, which allows to impose the trilinearity constraint per block, can still be applied. Moreover, an additional component was considered in the MCR Slicing decomposition. The trilinearity constraint was not applied to this fourth component in any of the three blocks. This is a way to handle some deviation from the ideal bilinear behavior of the system [18].

As previously, each block was individually sliced into five slabs, and then the fifteen slices were concatenated in a row-wise augmented multiblock structure to which MCR Slicing was applied. However, different from Dataset 1, the trilinearity constraint was imposed separately on each individual block since they are not expected to follow the same exponential behavior due to the illumination scheme applied. The results obtained for a four-component decomposition are shown in Fig. 6. As can be seen, these results translate a more complex behavior than the one observed for Dataset 1. The first three components, to which the trilinearity constraint was applied, are similar to the ones previously attributed to ConA (Fig. 6a) and DiBAC$_4$(3) (Fig. 6b and c). However, the time trace of the fourth component (dashed trace in Fig. 6e) shows a pattern that translates a clear deviation from the ideal

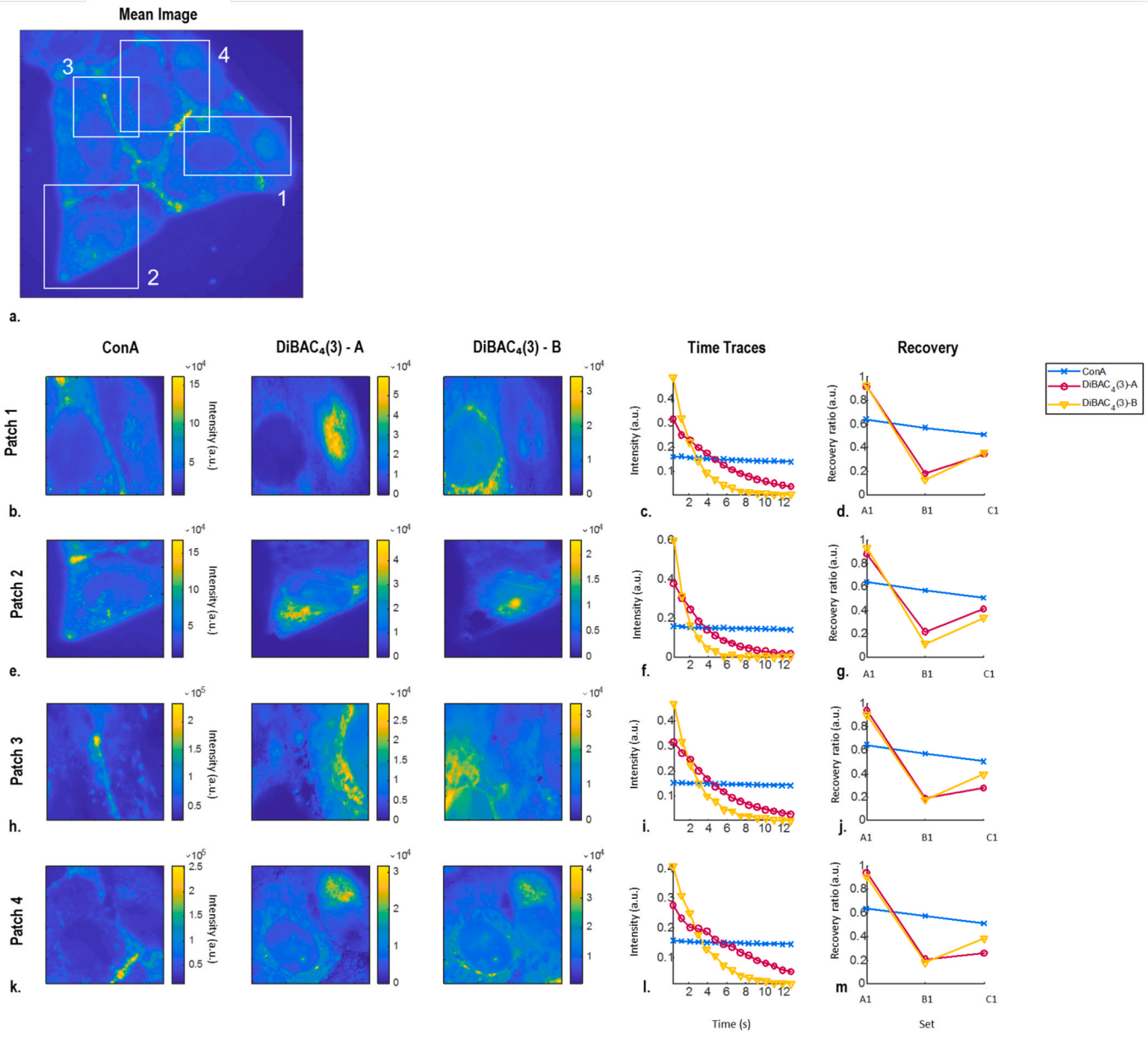

Fig. 4. Three component four-way PARAFAC Slicing decomposition of Dataset 1, replicated on different patches across the full field of view. **a.** Averaged image of the full field of view with the localization of the four patches highlighted. **b-d.** Distribution maps (**b**), attributed to ConA and $DiBAC_4(3)$ respectively, with the corresponding monoexponential time traces (**c**) and recovery ratio (**d**) of pure components retrieved from Patch 1, $r^2 = 99.83\%$. **e-h.** Reconstructed distribution maps, recovered time traces and recovery ratios for Patch 2 ($r^2 = 99.82\%$), Patch 3 ($r^2 = 99.79\%$) and Patch 4 ($r^2 = 99.87\%$), shown in similar fashion.

well-behaving exponential signal for the fluorophores, the corresponding distribution map (Fig. 6d) showing similarities with the one attributed to ConA (with some background contribution). Despite the difficulty in fully interpreting the complexity of the system, these results highlight the flexibility of MCR Slicing when faced with difficult analytical problems.

4. Conclusions

In this work we implemented a methodology for exploratory analysis and unmixing of fluorescence microscopy imaging data using Slicing and multilinear decomposition approaches, namely PARAFAC Slicing and MCR Slicing. In contrast to lifetime fitting methods (see *e.g.* Ref. [19]) where the model is thought *a priori* (before the data are even acquired), in the proposed methodology the hypothesis of exponential behavior comes from the data structure itself.

We applied this strategy to two samples of U2OS cells stained using both $DiBAC_4(3)$ and Concanavalin A - Alexa Fluor 488. Both samples have been acquired using a sequential illumination strategy in which several photodestruciton phases were interspersed by a fluorophore recovery phase. The laser power used during the photodestruction phases influences the characteristic decay time exihibited by each fluorophore, while the fluorescence recovery time determines which percentage of the total fluorophore molecules will be available for the next illumination phase (if the fluorophore shows the ability to recover).

In the first dataset, the illumination power was kept fixed, while the recovery time was increased between the photodestruction sections. This allowed both a trilinear MCR model and a quadrilinear PARAFAC model to be used to describe the dataset, yielding the characteristic time traces for each fluorophore, their associated distribution maps and the recovery ratio at the start of each photodestruction section. The analysis was repeated on several patches across the field of view yielding

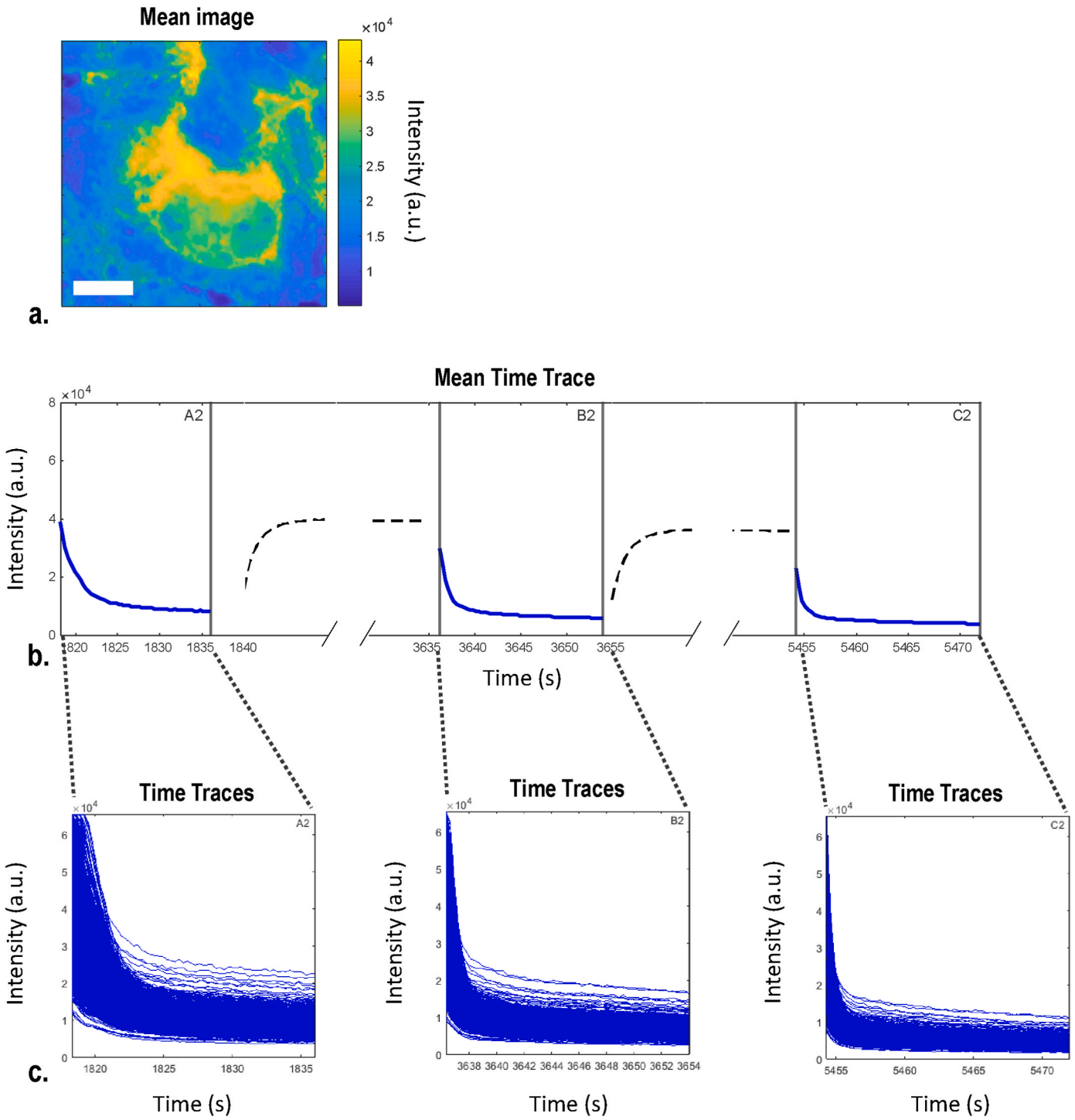

Fig. 5. Second U2OS cells dataset. **a.** Image averaged across all capture time. Image size 40 × 45 μm, scalebar 10 µm. **b.** Averaged time traces, shown to illustrate the illumination scheme: 18 s of photodestruction at 2.23 mW laser power for section A2, 30 minutes of fluorophore recovery, 18 s of photodestruction at 3.91 mW laser power for section B2, 30 minutes of fluorophore recovery, 18 s of photodestruction at 6.2 mW laser power for section C2. Only the photodestruction sections were used for the analysis. **c.** Time traces relative to the three photodestruction sections.

comparable results. Also, these quadrilinear models were obtained directly, without the use of previous assumptions or operator knowledge of the system, except for the overall structure of the dataset.

In the second dataset the laser power was increased in each photodestruction phase throughout the experiment. A clear perturbing effect was successfully dealt with by adding an additional component in the MCR Slicing model used to describe the dataset.

Multilinear Slicing has therefore been proven effective in the unmixing of photobleaching fluorescence imaging data using single-channel detection, and the several different approaches used showcased its ability to be effectively applied to a variety of experimental situations. Overall, this work provides future opportunities for the analysis of more complex multiplexed fluorescence imaging scenarios and for robust blind unmixing of fluorescence lifetime imaging (FLIM) data. In this context, comparison to other exploratory approaches could be performed, such as phasor analysis [20], which provides a graphical

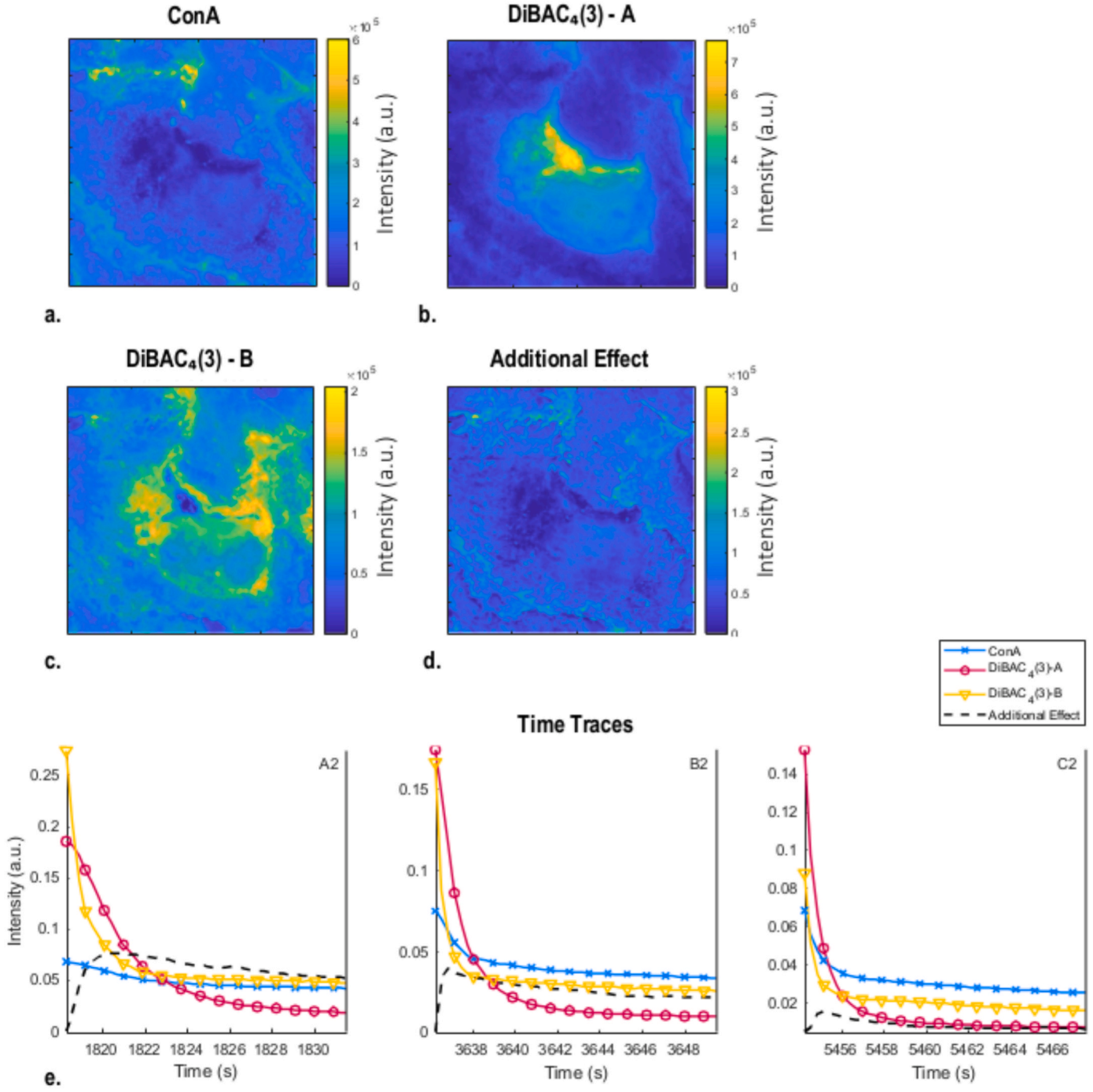

Fig. 6. Four component MCR Slicing decomposition of Dataset 2. **a-d.** Distribution maps; **e.** monoexponential time traces. LOF:4.65%, $r^2 = 99.78\%$.

representation of the pixel distribution in a polar plot to help distinguishing between different lifetime populations when different point clusters can be observed.

Funding

This work was supported by the International Associate Laboratory for High Performance Fluorescence Microscopy (HPFM) Univ. Lille-KU Leuven.

Credit author statement

Dario Cevoli: Methodology, Data analysis, Writing - Original Draft, Writing - Review & Editing. **Siewert Huguelier:** Experimental, Data acquisition, Writing - Review & Editing. **Robin Van den Eynde:** Experimental, Data acquisition, Writing - Review & Editing. **Olivier Devos:** Methodology. **Peter Dedecker:** Conceptualization, Writing - Review & Editing, Supervision. **Cyril Ruckebusch:** Conceptualization, Methodology, Writing - Review & Editing, Supervision.

Declaration of competing interest

The authors declare that they have no known competing financial interests or personal relationships that could have appeared to influence the work reported in this paper.

Acknowledgements

The authors thank Raffaele Vitale for fruitful discussion.

Appendix A

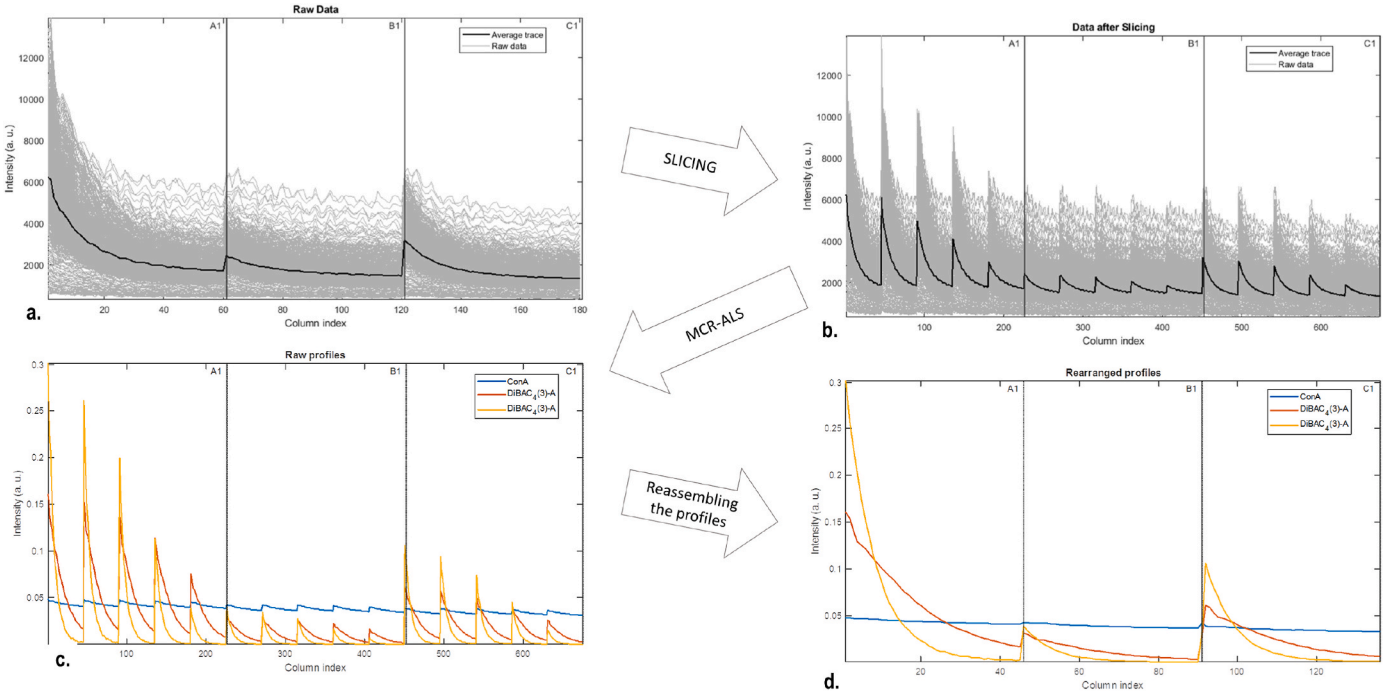

Fig. 7. Three component MCR Slicing on Datased 1. **a.** Raw data, were the three photodestruction blocks are concatenated. **b.** After each block is sliced (five slice are produced), the slices are concatenated row-wise and the sliced data is analyzed using MCR-ALS under trilinearity constrain. **c.** Full time traces of the three components extracted from the sliced data. **d.** The first slice for each block is shown.

References

[1] R. Neher, E. Neher, Optimizing imaging parameters for the separation of multiple labels in a fluorescence image, J. Microsc. 213 (2004) 46–62, https://doi.org/10.1111/j.1365-2818.2004.01262.x.

[2] S. Duwé, W. Vandenberg, P. Dedecker, Live-cell monochromatic dual-label sub-diffraction microscopy by mt-pcSOFI, ChemComm 53 (2017) 7242–7245, https://doi.org/10.1039/C7CC02344H.

[3] T. Roebroek, W. Vandenberg, F. Sipieter, S. Hugelier, C. Stove, J. Zhang, P. Dedecker, Simultaneous readout of multiple FRET pairs using photochromism, preprint, Biophys. J. (2021), https://doi.org/10.1101/2021.01.06.425528.

[4] S. Hugelier, R. Van den Eynde, W. Vandenberg, P. Dedecker, Fluorophore unmixing based on bleaching and recovery kinetics using MCR-ALS, Talanta 226 (2021) 122117, https://doi.org/10.1016/j.talanta.2021.122117.

[5] W. Windig, B. Antalek, Direct exponential curve resolution algorithm (DECRA) A novel application of the generalized rank annihilation method for a single spectral mixture data set with exponentially decaying contribution profiles, Chemometr. Intell. Lab. Syst. (1997) 14.

[6] H.T. Pedersen, R. Bro, S.B. Engelsen, Towards rapid and unique curve resolution of low-field NMR relaxation data: trilinear SLICING versus two-dimensional curve fitting, J. Magn. Reson. 157 (2002) 141–155, https://doi.org/10.1006/jmre.2002.2570.

[7] E. Sanchez, B.R. Kowalski, Tensorial resolution: a direct trilinear decomposition, J. Chemom. 4 (1990) 29–45.

[8] R. Bro, PARAFAC. Tutorial and applications, Chemometr. Intell. Lab. Syst. 38 (1997) 149–171, https://doi.org/10.1016/S0169-7439(97)00032-4.

[9] O. Devos, M. Ghaffari, R. Vitale, A. de Juan, M. Sliwa, C. Ruckebusch, Multivariate curve resolution slicing of multiexponential time-resolved spectroscopy fluorescence data, Anal. Chem. 93 (2021) 12504–12513, https://doi.org/10.1021/acs.analchem.1c01284.

[10] R. Bro, H.A. Kiers, A new efficient method for determining the number of components in parafac models, J. Chemom. 17 (2003) 274–286.

[11] R. Tauler, A. Smilde, B. Kowalski, Selectivity, local rank, three-way data analysis and ambiguity in multivariate curve resolution, J. Chemom. 9 (1995) 31–58, https://doi.org/10.1002/cem.1180090105.

[12] A. de Juan, J. Jaumot, R. Tauler, Multivariate Curve Resolution (MCR). Solving the mixture analysis problem, Anal. Methods 6 (2014) 4964–4976, https://doi.org/10.1039/C4AY00571F.

[13] G. Tomasi, R. Bro, PARAFAC and missing values, Chemometr. Intell. Lab. Syst. 75 (2005) 163–180, https://doi.org/10.1016/j.chemolab.2004.07.003.

[14] L. Rubio, L. Sarabia, M. Ortiz, Standard addition method based on four-way parafac decomposition to solve the matrix interferences in the determination of carbamate pesticides in lettuce using excitation–emission fluorescence data, Talanta 138 (2015) 86–99.

[15] R. Bro, P. Geladi, A. Smilde, Multi-way Analysis with Applications in the Chemical Sciences, John Wiley & Sons Ltd, 2004.

[16] R. Bro, N.D. Sidiropoulos, Least squares algorithms under unimodality and non-negativity constraints, J. Chemom. 12 (1998) 223–247.

[17] S.B. Engelsen, R. Bro, Powerslicing, J. Magn. Reson. 163 (2003) 192–197, https://doi.org/10.1016/S1090-7807(03)00125-3.

[18] B. Debus, M. Sliwa, H. Miyasaka, J. Abe, C. Ruckebusch, Multivariate curve resolution — alternating least squares to cope with deviations from data bilinearity in ultrafast time-resolved spectroscopy, Chemometr. Intell. Lab. Syst. 128 (2013) 101–110, https://doi.org/10.1016/j.chemolab.2013.08.001.

[19] P.J. Verveer, A. Squire, P.I. Bastiaens, Global analysis of fluorescence lifetime imaging microscopy data, Biophys. J. 78 (2000) 2127–2137.

[20] M.A. Digman, V.R. Caiolfa, M. Zamai, E. Gratton, The phasor approach to fluorescence lifetime imaging analysis, Biophys. J. 94 (2008) L14–L16.